Chapter 14
Trends in High Speed Interconnects: InP Monolithic Integration

Kevin Williams and Boudewijn Docter

14.1 Introduction

Performance has proved to be the primary driver for integrated circuit technology. Wafer scale integration is instrumental in removing assembly complexity and variability and enables sustained increases in the functionality, performance and circuit reliability while at the same time reducing size, power and cost [1, 2]. PIC-enabled products now outperform equivalent combinations of discrete components at the functional level for telecom systems. Digital coherent transceivers are a striking example of circuits which could not be produced cost-effectively in any other way [3]. Wavelength-multiplexed transceivers [4] and potentially optical packet switching circuits [5] may be expected to follow.

Yield has been improved through sustained technology development for InP-based epitaxial growth, fabrication processes and device design innovations. Killer defect densities have been driven down to levels comparable with silicon CMOS in the early 1990s [4] with Infinera reporting random killer defect densities in the range 0.5–1.25 cm^{-2} and functional yields as high as 70% for 440 element circuits [2]. Improved reliability becomes a key advantage for InP-integrated photonics technology as the performance-yield envelope is dominated by packaging and assembly. Strict design methodologies and tightly controlled, standardized processes have been essential. Vertically integrated corporations such as Infinera [4] and open access platforms such as JePPIX [6] have adopted methodologies for InP-based PICs which exhibit similarities to the CMOS electronic IC approach.

K. Williams (✉)
Institute for Photonic Integration, (COBRA), Technical University Eindhoven, Flux Building 9.067, 5612 AJ Eindhoven, The Netherlands
e-mail: k.a.williams@tue.nl

B. Docter
EFFECT Photonics BV, Torenallee 20, 5617 BC Eindhoven, The Netherlands
e-mail: boudewijndocter@effectphotonics.nl

F. Testa, L. Pavesi (eds.), *Optical Switching in Next Generation Data Centers*,
DOI 10.1007/978-3-319-61052-8_14

Scaling laws for InP-integrated photonics are similar to other thin film fabrication technologies like CMOS electronics and silicon photonics. Cost is defined by the market volumes, so an increased wafer size and fab throughput leads to a decreasing price-per-square-millimetre price [7]. Current volumes of photonic product are addressed with wafer sizes of 3″ and 4″, but as volumes increase, the cost advantages of moving to larger wafer sizes, increasing wafer batch sizes and levels of automation will appear. Integration becomes increasingly important as the volumes scale. Much as in electronics, costs will be dominated by test and assembly rather than wafer production providing the driver for further integration.

In this chapter, we review the InP integration techniques most relevant to current and future data interconnection. The InP building blocks are first reviewed, before integration methods, and compared. State-of-the-art devices and circuits are overviewed for direct detection and coherent communications. Components for transparent optical networking are addressed before considering trends in technology integration and wafer-scale assembly.

14.2 The Building Blocks

The rich diversity of InP components can be concisely described in terms of basic building blocks [6] which may be visualized through waveguide cross-sections. Figure 14.1 shows examples of basic building blocks from an open access InP-integrated photonics platform. The five different types of waveguide cross-sections are shown from left to right: (i) optical amplification and absorption, (ii) electro-optic phase modulation, (iii) shallow-ridge optical waveguiding, (iv) deep-ridge optical waveguiding and (v) polarization rotation. Enhanced performance is enabled through adjustments to the precise cross-section and process flow used. The power of monolithic integration is to create these building blocks in the same plane, on the same wafer and in the same process flow, making optical losses and reflections between components negligible.

Amplifiers are implemented through the simultaneous confinement of optical field and charge carriers within a separate confinement heterostructure. Figure 14.1 shows confinement of the optical field (white) in the SCH region (green) and with an additional active layer (red). Here a shallow-ridge waveguide is shown, but deep-ridge and buried heterostructures are also feasible. The function is implemented in a p-i-n diode structure with electronic contacting layers optimized for low electrical resistance and low optical losses. Operating in forward bias enables amplification, while reverse bias enables detector, electro-absorption modulators or a saturable absorber functions. The precise active layer structure can be optimized depending on the precise performance requirements and function. Both multi-quantum well (MQW) and bulk quaternary layer stacks consisting of either InGaAsP or InAlGaAs materials are possible, where the InAlGaAs materials generally provide better high-temperature operation properties.

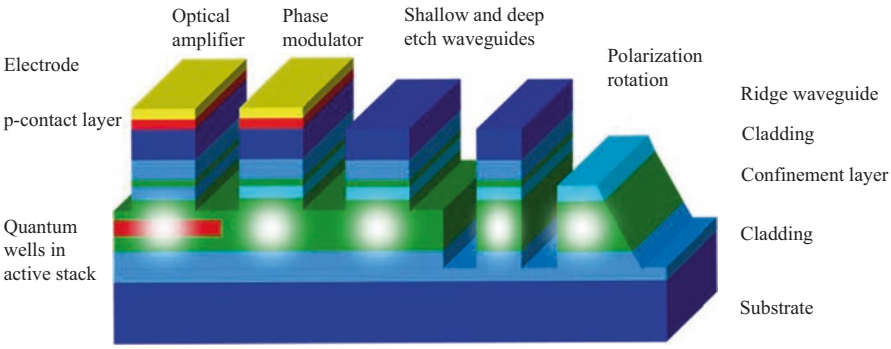

Fig. 14.1 Basic building blocks in InP photonic integration. From *left to right*, an amplifier or absorber, phase modulator, shallow-etch waveguide, deep-etch waveguides and polarization rotator

Phase modulators also use a p-i-n diode waveguide structure, but now the band gap is detuned from the signal wavelength. An increasing reverse bias applied across the junction induces a refractive index perturbation and an increasing phase shift. While bulk waveguide layers can be used, MQW InP modulators offer the most energy-efficient electro-optic conversion. Here the quantum-confined Stark effect (QCSE) is exploited. MQW layers within a PIN structure are designed with exciton absorption at a wavelength well below the desired operation wavelength. InP phase modulators require a larger detuning between signal and band gap wavelength than used for electro-absorption [8], and therefore Mach-Zehnder modulators that are built from these phase modulators have lower insertion loss. Phase modulators can also be operated in forward bias current injection mode. In this case the detuning needs to be smaller, and therefore the insertion loss is higher, but the phase tuning efficiency is very much increased. Typical values are 5 mA to tune 180 degrees in a 100 μm phase section. These phase shifters are commonly used inside laser cavities and distributed Bragg reflector (DBR) gratings to tune the lasing wavelength.

Shallow-ridge optical waveguides provide a means to connect active devices and create interferometric devices without the need to etch through the waveguide core. The removal of the contacting layers provides isolation between active components. Shallow etches may offer advantages in terms of reduced optical losses which arise from finite levels of surface roughness. As processing is increasingly well controlled, it is the dopants which dominate losses. In the absence of p-dopants, losses of below 0.5 dB/cm become feasible [9].

Deep-ridge optical waveguides provide a higher optical confinement and more compact optical bends. Bends with radii of order 20 μm have been reported [10, 11]. Deep-ridge structures are commonly used for multimode couplers, filters and arrayed waveguide grating de/multiplexers [12]. Distributed Bragg reflectors can also be implemented within the waveguides through a variation in the waveguide width, although it is more common to implement these in a separate epitaxial growth step.

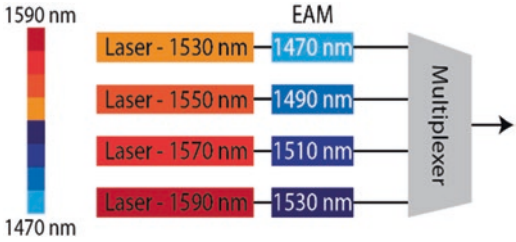

Fig. 14.2 The ability to create devices with different band edges (shown here in terms of wavelength) within the same high-density PIC. Concept for a wavelength-multiplexed transmitter [19]

Polarization rotators may be anticipated to provide the workhorse for a broad range of polarization-processing devices. Controlling the polarization within integrated circuits both accommodates variations in the input state of polarization and also allows an extra dimension for capacity scaling. Slanted side-wall waveguides have been long proposed to rotate the polarization [13]. So far, however, integrated polarization rotation devices have suffered from tight fabrication tolerances [14]. Recently a double-section polarization converter structure has been proposed and validated which has been able to correct for critical dimension variation [15, 16]. Combinations of phase modulators and polarization rotators may be implemented for conversion, splitting and combining, through to modulation [17] and analysis [18].

14.3 Monolithic Technology

Photonic-integrated circuits can be considered as multiple, interconnected, basic building blocks with varying epitaxial layers and waveguide cross-sections. Figure 14.2 shows an example schematic view for a WDM transmitter circuit implemented with a high number of different devices and band edges. Four methods stand out in the development of integrate devices with different band edges: vertically coupled epitaxial layers, quantum well intermixing, selective area growth and butt-joint integration. These methods are described below.

Vertically coupled layers have been used to enable the separate growth of active and passive integrated circuits, with notable examples in optical packet switch matrices [20], transceivers [21] and mode-matching elements [22]. The techniques have been extended most recently to enable the inclusion of InP devices on silicon photonic waveguides and facilitate efficient end-fire fibre coupling from PICs in general. The reliance on precision epitaxy and lithography impacts the yield-performance envelope, but this may be expected to improve with new generations of tooling in photonic circuit production. The physical size of tapers between elements will impact footprint and density. For some variants of silicon-based photonics where some of the active photonic building blocks originate from InP wafers, laser and amplifier integration becomes part of the assembly methodology.

Quantum well intermixing is typical of a broad range of post-growth techniques which allows the post-growth re-engineering of the band gap at the building block

level across the wafer [23–25]. The use of masked capping layers in combination with an annealing process allows a change in the composition and definition of the quantum wells and an associated change in emission wavelength. This enables the wavelength of the laser to be tuned relative to passive and absorber structures. Tunable lasers with electro-absorption modulators have been created with such an approach [26].

Selective area growth engineers the band edge during the epitaxial growth. Masking is used to locally enhance the growth rate. The dimensions of the mask define the thickness of the grown quantum wells and therefore the emission wavelength for quantum well lasers and band edge for modulators and detectors [27, 28]. Multiple band gaps can be defined across the same wafer to create combinations of building blocks with a higher level of functionality within one circuit. Lasers are readily incorporated with electro-absorption modulators [29, 30], and lasers can be integrated with passive components [31, 32]. Most recently, eight-channel distributed feedback laser arrays have been created with wavelength coverage from 1447 nm to 1602 nm. Threshold currents of 20 mA and output powers of up to 18 mW at 150 mA indicate efficient operation [33].

Butt-joint integration involves the etching and regrowth of different layer stacks across the wafer. The process can be repeated multiple times with the advantage that the epitaxial layer stack can be optimized at the building block level. For instance, the laser active regions require relatively few QWs for low threshold and high efficiency compared to the modulator where a high optical confinement factor is paramount [3]. This is also the most compact scheme with no inherent distance between the active and passive elements in the circuit [34] and very low reflections from the interfaces [35].

14.4 Transmitters

The techniques and building blocks used for converting electronic signals into the optical domain are increasingly diverse, reflecting a broad range of needs from today's links and networks. The most high-profile techniques in terms of research, development and deployment currently include:

- Directly modulated lasers (DML)
- Integrated laser modulators (ILM)
- Reflective semiconductor optical amplifiers (RSOA)
- Mach-Zehnder modulators (MZMs) and vector modulators

The functionality can be derived from a relatively small set of high-performance building blocks to enable optical gain, wavelength selection and phase modulation. The sophistication in integration technology scales as the module level performance increases to meet continued scaling demands in bandwidth, footprint and power consumption.

Directly modulated laser (DML) has been demonstrated for short, high grating strength distributed feedback lasers with high confinement factor InGaAlAs quantum wells. The cavity length directly influences modulation speed, with 25Gb/s demonstrated for 200 μm length devices and 40 Gb/s for 100 μm length devices [36]. High numbers of high-confinement wells ensure the high differential gain required for the modulation bandwidth, and a high grating strength ensures the low-threshold operation necessary. A current practical consideration for die handling necessitates the butt-joint connection of a passive waveguide for very short devices. Direct modulation bandwidths of 29GHz (3 dB) have been achieved, with a modulation efficiency of 4.85 GHz/mA$^{1/2}$, enabling 40-Gb/s transmission over 40-km-long single-mode fibre. The approach has most recently been extended to incorporate high electronic confinement 1.3-μm InGaAlAs active layers and the low-leakage ridge-shaped-buried heterostructures for a low threshold current of 5.6 mA at 85 °C. Clear eye openings and 10-km signal transmission have been claimed with 50Gb/s data transfer [37]. This already indicates suitability as a cost-effective light source in 400 GbE and OTU5 applications, and the integration with a passive section opens up possibilities for further functional integration. Passive feedback lasers offer an enhanced modulation bandwidth through the interaction with the feedback field. Integration is key in enabling precise phase control in a stable cavity. 40 Gb/s operation was demonstrated [38, 39] with a two-section device comprising a DFB laser and an integrated passive cavity.

Integrated laser modulators are most compactly implemented with the combination of DFB lasers and electro-absorption modulators. The initial challenge had been to control chirp and laser frequency in the presence of spurious back reflections [40], but significant progress has been made in terms of reflection suppression and modulation bandwidth. An InGaAlAs-based electro-absorption-modulated DFB laser has been operated with up to 56 Gb/s with low chirp and high output power. Lanes operate with extinction ratios of >9 dB at peak-to-peak voltages below 2 V and milliWatt mean modulated power levels in fibre. Such technology can be readily applied for O-band, C-band and L-band transmitters [41–43]. PAM4 coding has also been demonstrated with 56 GBaud/s symbol rates [44]. Beyond 100Gb/s becomes feasible with PAM8 coding at the 28 GBaud/s symbol rate [45] on a single wavelength.

Reflective SOAs have received renewed attention for access networking where the prospect of colourless operation enables enhanced network flexibility with simplified hardware. The amplified spontaneous emission (ASE) may be spectrum sliced, self-seeded or externally seeded by a remote transmitter. The limited modulation bandwidth can be accommodated with bit- and power-loaded discrete multitone (DMT) modulation to achieve data rates of order 30.7 Gbit/s with an externally seeded scheme [46]. Data rates of 28 Gb/s are independently achieved over 20 km with a directly modulated RSOA with the polar return-to-zero (RZ) N-ary pulse-amplitude modulation (PAM) format [47]. Leveraging advanced digital signal processing and digital to analogue conversion has enabled up to 40 Gb/s transmission [48].

Dense wavelength division multiplexing (DWDM) is exploited in the highest capacity PICs. Considerable progress has been made at Infinera, with 1700 components per chip and chip capacity exceeding 2 Tb/s in 2014 [49]. A high proportion of these devices are either energy-efficient InP modulators or lasers, ensuring an inherently scalable and complete chip-scale solution to ever-rising data rate requirements. Figure 14.3 shows the constituent parts in a WDM chip created using open access generic technology (jeppix.eu). From right to left, for the lower part of the die, there is a column of single-frequency distributed Bragg reflector lasers which connect to Mach-Zehnder modulators, an arrayed waveguide grating multiplexer, and then one single fibre-optic connection at the bottom left of the image. In this case, the device is designed according to a generic integration concept, using standardized building blocks, and is fabricated in a multiproject wafer run. The device delivers up to 4 dBm of optical power into the fibre with a modulation data rate of 12.5 Gbps per transmission channel [50].

Mach-Zehnder modulators (MZMs) in their simplest implementation enable on-off-keyed amplitude modulation. Lithium niobate modulators continue to set the standard in terms of modulation linearity and bandwidth, but the efficient quantum-confined Stark effect in InP MQW MZMs provides significantly smaller, submillimetre, interaction lengths compared to devices based on the Pockels effect [3]. InP offers the smallest and most energy-efficient, commercially produced modulators and already enables direct integration with the laser source [51, 52]. By detuning of the material band edge energy by 120 nm from the laser wavelength, InP Mach-Zehnder modulators are sufficiently broadband to allow operation over ninety 50-GHz-spaced DWDM channels [8]. The $V_{2\pi}$ modulation efficiencies are less than 5 V with an extinction ratio of more than 25 dB [53]. Enhanced optical confinement is able to improve efficiency further with the very high optical overlap achieved in substrate-removed devices: Values as low as 0.6 $V\pi$ mm have now been reported under push-pull drive [54, 55], and the longer devices have enabled bandwidth demonstrations to 67 GHz.

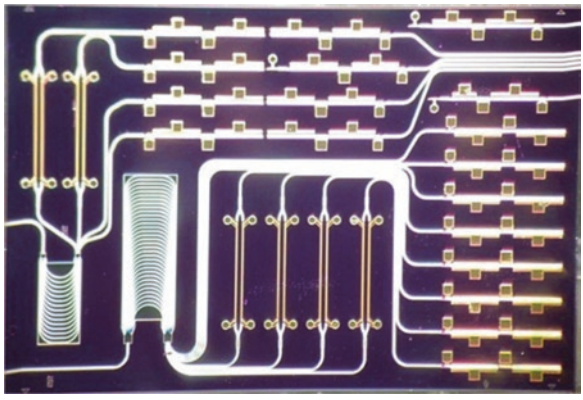

Fig. 14.3 Wavelength division multiplexed transmitter [50]

Vector modulators, also known as I&Q (in-phase and quadrature) modulators and nested MZMs, enable the simultaneous modulation of phase and amplitude. For higher data rates, the adoption of more complex modulation formats has contributed to the industry achievement of increasing capacity while satisfying the same link design rules as developed for 10 Gb/s transmission. The adoption of coherent technology, incorporating a local oscillator laser with a polarization and phase-diversity receiver, in combination with powerful CMOS digital signal processing (DSP), has further extended the achievable line rate and spectral efficiency. A dual-polarization (DP) I&Q modulator consisting of four MZMs can be employed to transmit 16-QAM modulation at 32 GBaud/s for a data rate of 200 Gb/s using a single wavelength [13]. Increased optical modulation complexity and loss can be compensated by the integration of optimally located SOA elements to achieve efficient optical gain, low noise figure and high saturation power. This is confirmed by operation within a CFP2 pluggable module [56]. An integrated tunable laser and vector modulator used with external polarization division multiplexing (PDM) emulation and digital coherent detection enabled data rates of 256 Gb/s per wavelength with PDM-16-QAM [57] and power dissipation as low as 3.2 W achievable [58]. The need for even greater capacity and spectral efficiency drives higher cardinality modulation formats such as PM-64QAM [59]. Further energy and footprint reductions are conceivable through, e.g. the integration of polarization optics, and innovative photonic design enables DAC-free operation, integrating traditionally electronic functionality within the PIC itself [60].

Integrated tuneable lasers leveraging sampled grating technologies have been an important enabler for telecom networking. The primary motivation was for inventory reduction, but considerable research interest has explored the potential for fast wavelength reconfigurability [61, 62]. For network reconfiguration, tunable laser products have been wavelength retuned within several nanoseconds with appropriate electronic control planes for the compensation of thermal crosstalk [63]. A programmable wavelength is an enabler for flex-grid and grid-less architectures, and the use of lasers with coherent systems enables optical filter-free detection. Integrating the lasers and modulators has the important manufacturability advantage of enabling full photonic testing at the wafer scale, to ensure the packaging of known good die. Performance parameters such as laser power, threshold and wavelength tuning characteristics as well as modulator switching voltage can be determined with wafer probe testing, before single dies are separated and packaged. Test components that have no function in the final application, such as test laser sources on WDM receiver chips, are now being designed into devices to get as much test and yield data before chips are committed to the packaging and assembly process.

Scaling to higher information densities requires a mitigation and suppression of thermal, optical and electronic crosstalk. The thermal crosstalk between active and passive components can limit the performance of integrated Mach-Zehnder (MZ) modulators operating at high radio frequencies and has been quantified by measuring the effects on the electro-optical response of neighbouring MZ modulators [64]. The role of substrate thickness is similarly important as this defines the relative proximity of the heat sink [65]. Thermal crosstalk can be reduced through the

incorporation of deep trenches [66]. Electrical crosstalk is also observed between interconnect lines and electro-optical phase shifters in photonic-integrated circuits. Crosstalk originates from radiative and substrate coupling between lines and from shared ground connections [67].

14.5 Receivers

The photodiodes at the heart of an optical receiver convert optical amplitude-modulated signals to analogue electronic waveform. The range of detectors which have been developed reflects the optimizations which can be made in terms of sensitivity, power handling and electrical energy use. The early emphasis in direct-detection, long-haul fibre optic links has driven ever more sensitive receivers, although more recently, short-reach and digital coherent links have required high operating optical powers. The shorter-reach links have focussed on energy reduction at the link level, and higher received optical powers can lead to energy savings through reduced electronic amplification in the receiver. The main classes of detector include:

- Waveguide P-I-N detectors
- Avalanche photodiodes (APD)
- Optically amplified receivers
- Unitravelling carrier detectors (UTC)
- Coherent detection

Waveguide P-I-N detectors provide a highly efficient, wide-band means to convert amplitude-modulated data into the electronic domain, but the sensitivity is ultimately limited by the thermal noise in the receiver and any dark current. Early experimental evidence indicated that high-speed response with bandwidths of 110 GHz [68] was feasible with waveguide integration, and theoretical estimates indicated that 200 GHz should be feasible with appropriate levels of fabrication control. The waveguide approach enables the simultaneous optimization of detection efficiency and bandwidth efficiency [69]. A 40Gbit/s PIN diode integrated with a transimpedance amplifier can achieve a sensitivity of −10.5 dBm at a BER of 10^{-9} [70]. Side-illuminated photodetectors show an improved high-power behaviour, as the absorption is distributed laterally into a larger length of a thinner absorption layer in a controlled manner, compared to perpendicular illuminated detectors. Line rates of 85Gb/s and bandwidths of 110GHz have been achieved on semi-insulating substrates [71]. Ultimately PIN photodiodes will show saturation due to large densities of carriers generated in the depletion region [72].

Avalanche photodiodes are implemented with waveguides to achieve both high-speed performance and high responsivity through the exploitation of internal gain [72, 73]. A typical improvement of the photoreceiver sensitivity would be 5–10 dB compared with PIN photodiodes [71, 74]. Waveguide-integrated devices with sensitivity of -19 dBm at 40 Gb/s have been demonstrated [75, 76].

Waveguide integration also enables the further integration with other photonic components. Progress in epitaxial growth and specifically techniques with low residual doping and precise control of heterostructure interfaces have been instrumental in optimizing detectors, and this is particularly true for APDs where particularly high electric fields are required for avalanche gain. APD performances are related to electron and hole ionization coefficients in the multiplication region. Very low-noise APDs were demonstrated using a wide range of very thin avalanche layers, including InP, Al_x $In_{1-x}As$, GaAs and $Al_xGa_{1-x}As$.

Optically preamplified receivers with an SOA-PIN combination can enhance the sensitivity of a PIN detector to −17.5 dBm at 40 Gb/s [77]. The combination of optimized SOA preamplification and TIA design enables a large responsivity of 44 A/W, a polarization dependence below 2 dB, a low noise figure of 8.5 dB and a 3-dB bandwidth of 35 GHz [78]. Recently a 40-Gb/s photoreceiver module with differential outputs designed for short-reach applications such as access network and data centre interconnect was reported [79]. It consists of an InP semiconductor optical amplifier monolithically integrated with a p-i-n (SOA-PIN) photodiode, co-packaged with an InP linear transimpedance amplifier (TIA) and a matching circuit between the SOA-PIN and the TIA in order to increase the cutoff frequency. The module exhibits a − 3 dB bandwidth of 43 GHz, a single-ended optoelectrical conversion gain of 10,000 V/W for an optical input power of −25 dBm and a record sensitivity of −22.5 dBm at a bit error rate of 10^{-9} at 40 Gb/s in non-return-to-zero on/off -keying operation (Fig. 14.4).

Unitravelling carrier photodiodes (UTC) offer a means to scale in power and bandwidth. Unipolar photodiodes offer a particularly powerful structure to reduce space charge effect limitations since they use only electrons as active carriers [71]. High-speed unitravelling carrier photodiode has been demonstrated for 100 Gbit/s applications with a 3 dB bandwidth exceeding 110 GHz, a dark current of 1 nA and a peak saturation current of about 30 mA at −2 V [80]. When monolithically integrated with a semiconductor optical amplifier (SOA), a 95 GHz 3 dB bandwidth is still feasible with 8 dB noise figure and a polarization-dependent loss of 1–2 dB. The SOA integration enables a 95 A/W peak responsivity corresponding to record gain-bandwidth product of 6.1 THz [81]. UTC technology has also been extended to

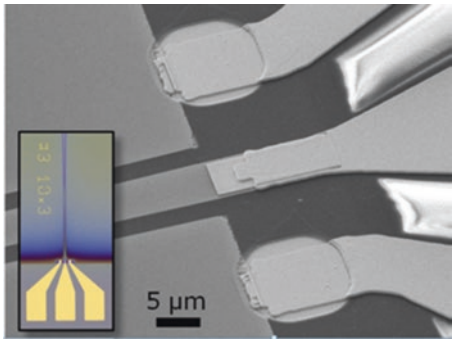

Fig. 14.4 UTC detector with >67 GHz bandwidth using InP membrane on silicon (IMOS) technology [83]

continuous-wave terahertz (THz) signal generation at 1.25 THz [82]. Integration of high-speed UTC devices with the substrate-free IMOS InP-membrane-on-silicon platform also enables integration with surface grating couplers and a route to high-density integration [83]. The higher optical confinement ensures a smaller cross-section, smaller bend radii, the possibility to use high-contrast reflectors for cavities and a route to smaller and denser packed devices. For the case of the photodiodes, a 150 nm thin p-type doped InGaAs layer is used both as the absorption layer and as the p-contact layer. The photogenerated holes are collected directly by the p-contact, while the electrons travel to the non-intentionally doped depletion region. The thickness of the p-layer is chosen as a trade-off between the optical absorption coefficient for efficiency and the electron transit time for bandwidth.

Coherent detection requires further integration, implementing the mixers with near-identical, ground-isolated, photodiodes to enable phase-sensitive detection and a richer range of bandwidth-efficient modulation formats. InP-based MMI (multimode interferometer)-mixer chip has been integrated with photodiodes by the butt-joint process to achieve high responsivity in a chip size of 2.0 mm × 5.1 mm. The 3 dB bandwidth is more than 20 GHz, and uniform characteristics of over four PDs have been achieved to enable 100Gb/s operation [84]. InP coherent receiver chip with the highest reported responsivity (0.15A/W) together with excellent RF bandwidth (32GHz) and 4 × 4 MMI width fabrication control (< ±60 nm 90% population) provides a highly manufacturable receiver for pluggable CFP2 modules [85]. InP offers an attractive and manufacturable platform for size and cost reduction as well as a common platform for full transceiver (laser, transmitter and receiver) integration.

14.6 Optical Switching

The energy and latency cost converting signals back and forth between the electrical and optical domain has long motivated R&D into optical switching technologies. While wavelength-selective switches, photonic switches and reconfigurable optical add-drop multiplexers are now an established part of the network, the technologies so far deployed have been operated as circuit switches. This is primarily a technology limitation. Microelectro-mechanical systems are widely used to provide high connectivity switching fabrics with hundreds of fibre connections. These approaches use free-space imaging of fibre arrays onto two-dimensional arrays of voltage-actuated micromechanical switch elements. This approach can be energy efficient as the low switch actuation power and optical power loss are both loss, and the devices can be transparent to bandwidth, enabling the routing of many tens of high bandwidth channels. However the actuation times, the requirement for power levelling and physical size continue to pose system implementation challenges. A rich vein of InP PIC research has sort to exploit nanosecond switch actuation, on-chip levelling and chip-scale implementation to enable reduced latency networking [86]. Switch architectures are primarily aligned to photonic switches with broadband

any-port-to-any-port routing and wavelength-selective switches. Multi-degree ROADMs may be implemented with combinations of the two architectures.

Photonic switches have been implemented at the chip scale using InP PICs with connectivities ranging 1 × 100 and 16 × 16. Single-input-port, integrated, phased-array optical switches offer a high port-count scalability and broad spectral coverage and can be used as building blocks of large-scale optical routers. Single stages of a 1 × 16 switch feature wavelength-independent nanosecond switching characteristics [87]. Scaling to 1 × 100 is demonstrated with an active-passive integration technology and a two-stage phase array interferometric switch. The inclusion of active SOA gates on the output enables an enhanced switch extinction [88] and the possibility for gain compensation. Such circuits have even been used to enable optical buffering experiments [89]. The implementation of multiple arrayed waveguides with shared free-space regions has also been explored with the creation of a strictly nonblocking 8 × 8 switch for high-speed, WDM optical interconnection [90]. The circuit consists of over 200 functional devices such as star couplers, phase shifters and avoided waveguide crossings. C-band operation with extinction ratio performance of more than 20 dB was achieved with nanosecond reconfiguration times. N × N switching matrices have also been implemented with combinations of Mach-Zehnder interferometers and SOA gates for 8 × 8 switch fabrics [91]. Broadcast and select architectures have been implemented in multiple stages to enable higher levels of connectivity in 16 × 16 fabrics [11, 92].

Reconfigurable optical packet switches enable per wavelength routing between multiple ports. InP PICs have been created using filter elements such as chained Mach-Zehnder interferometers [93], cross-point matrix implementations of third-order ring resonators [94] and arrayed waveguide grating-based wavelength selectors [95]. Wavelength selector circuits have also been implemented in parallel on the same die [96]. The demonstrated nanosecond switching of high line-rate data using such switches has provided a powerful means of enabling packet level routing at the chip level. Many-to-many connectivity with wavelength granularity becomes feasible with the combination of shuffle networks and parallel wavelength selectors. An example circuit is shown in Fig. 14.5 with eight-input to

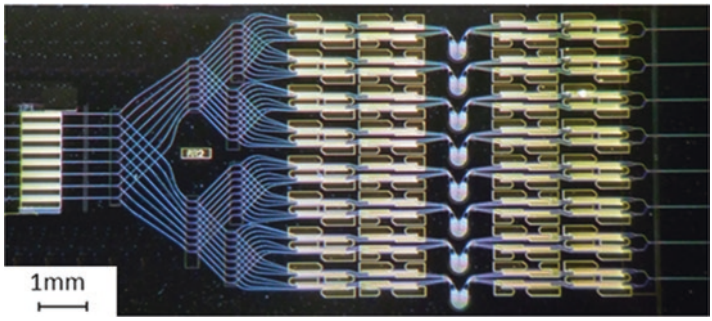

Fig. 14.5 Reconfigurable optical packet switch operating on eight input fibres (*left*), eight wavelength channels and eight output fibres (*right*) [5]

eight-output connectivity with cyclic arrayed waveguide grating routers operating on eight individual wavelengths or combs of wavelengths [5]. Dynamic routing has been demonstrated with real-time path reallocation with 16 channels with microsecond time slots [97].

14.7 Outlook

InP-integrated photonics scales along the same trajectory as other wafer-scale technologies. An increased production volume can be expected to lead to further yield improvements and cost reductions. The low-energy requirement from quantum-well-based building blocks enables shorter components with enhanced packing density for a given thermal load and chip area. This provides an important route to very high-density integration for terabit-class transmitters, receivers and routing circuits. Progress over the last decades has already led to the observation of a Moore's Law in photonic integration [98]. Indium phosphide membrane on silicon technology [99] may be expected to lead to a further step in miniaturization through high-confinement, ultradense InP optoelectronics for further footprint and energy reductions.

The package for PICs currently requires optomechanical connections, electronic connections and thermal management, each of which adds losses and cost. In telecommunications, the achievable data rate for a given link outweighs cost. For the data centre interconnect, data rate, cost and energy use are all critically important. Packages will become smaller with increasing levels of electronics co-packaged with the PIC. New methods to enable relaxed precision assembly will be critical. New techniques for automated optical alignment [100, 101] and reduced complexity electronic connection [100] become areas of active research.

Systems integration will become critical. Matching electronic and photonic design – co-design – and designing for uncooled (high temperature) operation are expected to have a major impact on both energy use and also assembly cost. As with electronic ICs, costs are initially dominated by auxiliary components, package and test, rather than the enabling chip itself. Here InP has a striking advantage. The monolithically integrated light sources already enable wafer-scale self-test. Uniquely, the lasers and amplifiers are created within one chip with high-performance multi-quantum well modulators, detectors and passives without introducing assembly steps between photonic devices. The epitaxial growth of energy-efficient multi-quantum wells and the use of thermally conductive waveguide cladding layers offer important energy efficiency advantages. Butt-joint integration allows component packing at the density limit, without the use of adiabatic tapers or extra-thick cladding layers. Other platforms offer subsets of devices and therefore may be assembled with other platforms in the packaged part, but the monolithic approach feasible for InP PICs ensures a chip-scale solution for sustained year-on-year scaling.

Acknowledgements Past and present members of the Institute for Photonic Integration, formerly known as the COBRA institute, are thanked for their stimulating contributions in the preparation of this chapter. The authors are also grateful to partners in JePPIX – the Joint European Platform for Photonic Integrated Components and Circuits – for their insights. Research projects which have had a particular input include Paradigm, Phastflex, GetPICs, WIPE, Photronics and Smartlight.

References

1. C.R. Doerr, K. Okamoto, Planar lightwave circuits in fiber-optic communications, in *Optical Fiber Telecommunications V A (Fifth Edition) Volume A: Components and Subsystems*, ed. by I. P. Kaminow, T. Li, A. E. Willner (Eds), (Elsevier, Amsterdam, 2008)
2. R. Nagarajan, M. Kato, J. Pleumeekers, P. Evans, S. Corzine, S. Hurtt, A. Dentai, S. Murthy, M. Missey, R. Muthiah, R.A. Salvatore, C. Joyner, R. Schneider, M. Ziari, F. Kish, D. Welch, InP photonic integrated circuits. Invited Paper, IEEE J. Sel. Top. Quantum Electron. **16**(5), 1113 (2010)
3. R.A. Griffin, S.K. Jones, N. Whitbread, S.C. Heck, L.N. Langley, InP Mach–Zehnder modulator platform for 10/40/100/200-Gb/s operation. Invited Paper, IEEE J. Sel. Top. Quantum Electron. **19**(6), 3401209 (2013)
4. F. Kish, R. Nagarajan, D. Welch, et al., From visible light-emitting diodes to large scale III-V photonic integrated circuits. Proc. IEEE **101**(10), 2255–2270 (2013)
5. R. Stabile, A. Rohit, K.A. Williams, Monolithically integrated 8×8 space and wavelength selective cross-connect. J. Lightwave Technol. **32**(2), 201 (2014)
6. M.K. Smit et al., An introduction to InP-based generic integration technology. Semicond. Sci. Technol. **29**(8), 083001–081/41 (2014)
7. JePPIX roadmap http://www.jeppix.eu/document_store/JePPIXRoadmap2015.pdf, 2015
8. R.A. Griffin, B. Pugh, J. Fraser, I.B. Betty, K. Anderson, G. Busico, C. Edge, T. Simmons, Compact, high power, MQW InP Mach-Zehnder transmitters with full-band tunability for 10 Gb/s DWDM. 4, 903–904.proceedings European Conference on Optical Communications (2005)
9. D. d'Agostino, G. Carnicella, C. Ciminelli, H.P.M.M. Ambrosius, M.K. Smit, Design of a compact high-performance InP ring resonator. Proceedings MEPHISTO 2014
10. R. Stabile, K.A. Williams, Relaxed dimensional tolerance whispering gallery microbends. J. Lightwave Technol. **29**(12), 2011 (1892)
11. R. Stabile, A. Albores-Mejia, K.A. Williams, Monolithic active-passive 16 × 16 optoelectronic switch. Opt. Lett. **37**(22), 4666 (2012)
12. K.A. Williams, E.A.J.M. Bente, D. Heiss, Y. Jiao, K. Ławniczuk, X.J.M. Leijtens, J.J.G.M. van der Tol, M.K. Smit, InP photonic circuits using generic integration. Photon. Res. **3**(5), B60–B68 (2015)
13. H. el-Refaei, D. Yevick, T. Jones, Slanted-rib waveguide InGaAsP–InP polarization converters. J. Lightwave Technol. **22**(5), 1352 (2004)
14. M. Zaitsu, T. Tanemura, Y. Nakano, Numerical study on fabrication tolerance of half-ridge InP polarization converters. IEICE Trans. Electron. **97-C**(7), 731 (2014)
15. D.O. Dzibrou, J.J.G.M. van der Tol, M.K. Smit, Improved fabrication process of low-loss and efficient polarization converters in InP-based photonic integrated circuits. Opt. Lett. **38**(7), 1061 (2013)
16. D.O. Dzibrou, J.J.G.M. van der Tol, M.K. Smit, Tolerant polarization converter for InGaAsP-InP photonic integrated circuits. Opt. Lett. **38**(18), 3482 (2013)
17. M.A. Naeem, M. Haji, B.M. Holmes, D.C. Hutchings, J.H. Marsh, A.E. Kelly, Generation of high speed polarization modulated data using a monolithically integrated device. IEEE J. Sel. Top. Quantum Electron. **21**(4), 3400205 (2015)
18. S. Ghosh, Y. Kawabata, T. Tanemura, Y. Nakano, Integrated Stokes vector analyzer on InP. Paper WD4–4, proceedings OECC/PS (2016)

19. M. Trajkovic, High speed electro-absorption modulator: a step towards high performance and high density PICs. Fotonica Magazine (2016)
20. S.C. Lee, R. Varrazza, S. Yu, Advanced optical packet switching functions using active vertical-couplers-based optical switch matrix. J. Sel. Top. Quantum Electron. **12**(4), 817–827 (2006)
21. V. Tolstikhin, Multi-guide vertical integration in InP: PIC technology for cost-sensitive applications. Proceedings Conference on Lasers and Electro-Optics Pacific Rim (2013)
22. I. Moerman, P.P. van Daele, P.M. Demeester, A review on fabrication technologies for the monolithic integration of tapers with III-V semiconductor devices. IEEE J. Sel. Top. Quantum Electron. **3**(6), 1308–1320 (1997)
23. S. McDougall, O. Kowalski, C. Hamilton, F. Camacho, B. Qiu, M. Ke, R. De La Rue, A. Bryce, J. Marsh, Monolithic integration via a universal damage enhanced quantum-well intermixing technique. IEEE J. Sel. Top. Quantum Electron. **4**(4), 636–646 (1998)
24. A. McKee, C.J. McLean, G. Lullo, A.C. Bryce, R.M. Rue, J.H. Marsh, Monolithic integration in InGaAs-InGaAsP multiple-quantum-well structures using laser intermixing. IEEE J. Quantum Electron. **33**, 45–55 (1997)
25. E.J. Skogen, J.W. Raring, G.B. Morrison, C.S. Wang, V. Lal, M.L. Masanovic, L.A. Coldren, Monolithically integrated active components: A quantum-well intermixing approach. J. Sel. Top. Quantum Electron. **11**(2), 343–355 (2005)
26. J.W. Raring, E.J. Skogen, L.A. Johansson, M.N. Sysak, S.P. DenBaars, L.A. Coldren, Widely tunable negative-chirp SG-DBR laser/EA-modulated transmitter. J. Lightwave Technol. **23**(1), 80–86 (2005)
27. R. Bhat, Non-planar and masked-area epitaxy by organometallic chemical vapour deposition. Semicond. Sci. Technol. **8**, 984–993 (1993)
28. M. Gibbon, J.P. Stags, C.G. Cureton, E.J. Thrush, C.J. Jones, Selective-area low-pressure MOCVD of GalnAsP and related materials on planar InP substrates. Semicond. Sci. Technol **8**, 998–1010 (1993)
29. N. Dupuis, J. Décobert, C. Jany, F. Alexandre, A. Garreau, R. Brenot, N. Lagay, F. Martin, D. Carpentier, J. Landreau, F. Pommereau, F. Poingt and C. Kazmierski, Selective area growth engineering for 80 nm spectral range AlGaInAs 10 Gbit/s remote amplified modulator. Proceedings indium phosphide and related materials (2008)
30. H. Debrégeas, J. Decobert, N. Lagay, R. Guillamet, D. Carrara, O. Patard, C. Kazmierski, R. Brenot, Selective-area-growth technology for flexible active building blocks. Proceedings advanced photonics congress, IM2A.3 (2012)
31. J. Décobert, N. Dupuis, P.Y. Lagrée, N. Lagay, A. Ramdane, A. Ougazzaden, F. Poingt, C. Cuisin, C. Kazmierski, Modeling and characterization of AlGaInAs and related materials using selective area growth by metal-organic vapor phase epitaxy. J. Cryst. Growth **298**, 28–31 (2007)
32. J. Decobert, G. Binet, A.D.B. Maia, P.Y. Lagrée, Christophe Kazmierski, "AlGaInAs MOVPE selective area growth for photonic integrated circuits". Adv Opt Technol **4**, 2 (2015)
33. F. Soares, M. F. Baier, Z. Zhang, T. Gaertner, D. Franke, J. Decobert, M. Achouche, D. Schmidt, M. Moehrle, N. Grote, M. Schell, 155 nm-span multi-wavelength DFB laser array fabricated by selective area growth. Paper MoC4–4. Proceedings compound semiconductor week (2016)
34. J. Binsma, P. Thijs, T. van Dongen, E. Jansen, A. Staring, G. van den Hoven, L. Tiemeijer, Characterization of butt-joint InGaAsP waveguides and their application to 1310 nm DBR-type MQW gain-clamped semiconductor optical amplifiers. IEICE Trans. Electron. **E80-C**, 675–681 (1997)
35. Y. Barbarin, E.A.J.M. Bente, C. Marquet, E.J.S. Leclère, J.J.M. Binsma, M.K. Smit, Measurement of reflectivity of butt-joint active–passive interfaces in integrated extended cavity lasers. Photon. Technol. Lett. **17**(11), 2265–2267 (2005)
36. W. Kobayashi, T. Tadokoro, T. Fujisawa, N. Fujiwara, T. Yamanaka and F. Kano, 40-Gbps direct modulation of 1.3-μm InGaAlAs DFB laser in compact TO-CAN package. Paper OWD2, proceedings optical fiber communications conference (2011)

37. K. Nakahara, Y. Wakayama, T. Kitatani, T. Taniguchi, T. Fukamachi, Y. Sakuma, S. Tanaka, Direct modulation at 56 and 50 Gb/s of 1.3-μm InGaAlAs ridge-shaped-BH DFB lasers. IEEE Photon. Technol. Lett. **27**(5), 534–536 (2015)
38. U. Troppenz, J. Kreissl, M. Möhrle, C. Bornholdt, W. Rehbein, B. Sartorius, I. Woods, M. Schell, 40 Gbit/s directly modulated lasers: Physics and application. 7953, 79530F-1–79530F-10, proceedings SPIE (2011)
39. J. Kreissl, V. Vercesi, U. Troppenz, T. Gaertner, W. Wenisch, M. Schell, Up to 40-Gb/s directly modulated laser operating at low driving current: Buried-heterostructure passive feedback laser (BH-PFL). IEEE Photon. Technol. Lett. **24**(5), 362 (2012)
40. J.A.J. Fells, M.A. Gibbon, G.H.B. Thompson, I.H. White, R.V. Penty, A.P. Wright, R.A. Saunders, C.J. Armistead, E.M. Kimber, Chirp and system performance of integrated laser modulators. IEEE Photon. Technol. Lett. **7**(11), 1279 (1995)
41. M. Theurer, Y. Wang, L. Zeng, U. Troppenz, G. Przyrembel, A. Sigmund, M. Moehrle, M. Schell, 2×56 Gb/s from a double side electroabsorption modulated DFB laser. Paper Tu3D.6 OFC (2016)
42. M. Theurer, H. Zhang, Y. Wang, W. Chen, L. Zeng, U. Troppenz, G. Przyrembel, A. Sigmund, M. Moehrle, M. Schell, 2×56 Gb/s from a double side electroabsorption modulated DFB laser and application in novel optical PAM4 generation. J. Lightwave Technol. Accepted for publication 03 August 2016
43. M. Theurer, G. Przyrembel, A. Sigmund, W.D. Molzow, U. Troppenz, M. Mohrle, 56 Gb/s L-band InGaAlAs ridge waveguide electroabsorption modulated laser with integrated SOA. Phys. Status Solidi A **213**(4), 970–974 (2016)
44. M.A. Mestre, H. Mardoyan, C. Caillaud, R. Rios-Muller, J. Renaudier, P. Jenneve, F. Blache, F. Pommereau, J. Decobert, F. Jorge, P. Charbonnier, A. Konczykowska, J.Y. Dupuy, K. Mekhazni, J.F. Paret, M. Faugeron, F. Mallecot, M. Achouche, S. Bigo, Compact InP-based DFB-EAM enabling PAM-4 112 Gb/s transmission over 2 km. J. Lightwave Technol. **34**(7), 1572 (2016)
45. U. Troppenz, M. Narodovitch, C. Kottke, G. Przyrembel, W.D. Molzow, A. Sigmund, H.G. Bach, M. Moehrle, 1.3 μm electroabsorption modulated lasers for PAM4/PAM8 single channel 100 Gb/s. Paper Th-B2–5, Montpelier, international conference on indium phosphide and related materials (2014)
46. S.A. Gebrewold, R. Brenot, R. Bonjour, A. Josten, B. Baeuerle, D. Hillerkuss, C. Hafner, J. Leuthold, Colorless low-cost RSOA based transmitters optimized for highest capacity through bit- and power-loaded DMT. Proceedings optical fiber communications conference, Tu2C.4 (2016)
47. H.K. Shim, H. Kim, Y.C. Chung, Effects of electrical and optical equalizations in 28-Gb/s RSOA-based WDM PON. Photon. Technol. Lett. **28**(22), 2537–2540 (2016)
48. B.Y. Cao, M.L. Deng, R.P. Giddings, X. Duan, Q.W. Zhang, M. Wang, J.M. Tang, RSOA intensity modulator frequency chirp-enabled 40Gb/s over 25km IMDD PON systems. Proceedings optical fiber communications conference, W1J.3 (2015)
49. J. Summers, T. Vallaitis, P. Evans, M. Ziari, P. Studenkov, M. Fisher, J. Sena, A. James, S. Corzine, D. Pavinski, J. Ou-Yang, M. Missey, D. Gold, W. Williams, M. Lai, D. Welch, F. Kish, Monolithic InP-based coherent transmitter photonic integrated circuit with 2.25 Tbit/s capacity. Electron. Lett. **50**(16), 1150 (2014)
50. K. Ławniczuk, C. Kazmierski, J.G. Provost, M.J. Wale, R. Piramidowicz, P. Szczepanski, M.K. Smit, X.J.M. Leijtens, InP-based photonic multiwavelength transmitter with DBR laser array. Photon Technol. Lett. **25**(4), 352 (2013)
51. J.E. Zucker, K.L. Jones, B.I. Miller, U. Koren, Miniature Mach-Zehnder InGaAsP quantum well waveguide interferometers for 1.3 μm. IEEE Photon. Technol. Lett. **2**(1), 32–34 (1990)
52. J.E. Zucker, K.L. Jones, M.A. Newkirk, R.P. Gnall, B.I. Miller, M.G. Young, U. Koren, C.A. Burrus, B. Tell, Quantum well interferometric modulator monolithically integrated with 1.55 μm tunable distributed Bragg reflector laser. Electron. Lett. **28**(20), 1888–1889 (1992)

53. S.C. Heck, S.K. Jones, R.A. Griffin, N. Whitbread, P.A. Bromley, G. Harris, D. Smith, L.N. Langley, T. Goodhall, Miniaturized InP dual I&Q Mach Zehnder modulator with full monitoring functionality for CFP2. Proceedings European conference on optical communications, paper Tu.4.4.2 (2014)
54. S. Dogru, N. Dagli, 0.77-V drive voltage electro-optic modulator with bandwidth exceeding 67 GHz. Opt. Lett. **39**(20), 6074 (2014)
55. S. Dogru, N. Dagli, 0.2V drive voltage substrate removed electro-optic Mach-Zehnder modulators with MQW cores at 1.55 μm. IEEE/OSA J. Lightwave Technol. **32**(3), 435–439 (2014)
56. R.A. Griffin, N. D. Whitbread, S.K. Jones, S.C. Heck, P. Firth, D. Govan, T. Goodall, InP coherent optical modulator with integrated amplification for high capacity transmission. Paper Th4E.2, proceedings optical fiber communications conference (2015)
57. S. Chandrasekhar, X. Liu, P.J. Winzer, J.E. Simsarian, R.A. Griffin, Compact all-InP laser-vector-modulator for generation and transmission of 100-Gb/s PDM-QPSK and 200-Gb/s PDM-16-QAM. J. Lightwave Technol. **32**(4), 736 (2014)
58. T. Tatsumi, N. Itabashi, T. Ikagawa, N. Kono, M. Seki, K. Tanaka, K. Yamaji, Y. Fujimura, K. Uesaka, T. Nakabayashi, H. Shoji, S. Ogita, A compact low-power 224-Gb/s DP-16QAM modulator module with InP-based modulator and linear driver ICs. Paper Tu3H.5, proceedings optical fiber communications conference (2014)
59. W. Forysiak, D.S. Govan, Progress toward 100-G digital coherent pluggables using InP-based photonics. J. Lightwave Technol. **32**(16), 2925 (2014)
60. A. Aimone, I.G. Lopez, S. Alreesh, P. Rito, T. Brast, V. Hohns. G. Fiol, M. Gruner, J. Fischer, J. Honecker, A. Steffan, D. Kissinger, A.C. Ulusoy, M. Schell, DAC-free ultra-low-power dual-polarization 64-QAM transmission with InP IQ segmented MZM module. Postdeadline paper Th5C.6 proceedings optical fiber communications conference (2016)
61. L.A. Coldren, G.A. Fish, Y. Akulova, J.S. Barton, L. Johansson, C.W. Coldren, Tunable semiconductor lasers: A tutorial. J. Lightwave Technol. **22**(1), 193–202 (2004)
62. A.J. Ward, D.J. Robbins, G. Busico, E. Barton, L. Ponnampalam, J.P. Duck, N.D. Whitbread, P.J. Williams, D.C.J. Reid, A.C. Carter, M.J. Wale, Widely tunable DS-DBR laser with monolithically integrated SOA: Design and performance. J. Sel. Top. Quantum Electron. **11**(1), 149 (2005)
63. J.E. Simsarian, M.C. Larson, H.E. Garrett, H. Xu, T.A. Strand, Less than 5-ns wavelength switching with an SG-DBR laser. Photon. Technol. Lett. **18**(4), 565 (2006)
64. G. Gilardi, W. Yao, M.K. Smit, M.J. Wale, Observation of dynamic extinction ratio and bit error rate degradation due to thermal effects in integrated modulators. J. Lightwave Technol. **33**(11), 2199 (2015)
65. G. Gilardi, W. Yao, H.R. Haghighi, M.K. Smit, M.J. Wale, Substrate thickness effects on thermal crosstalk in InP-based photonic integrated circuits. J. Lightwave Technol. **32**(17), 3061 (2014)
66. G. Gilardi, W. Yao, H.R. Haghighi, X.J.M. Leijtens, M.K. Smit, M.J. Wale, Deep trenches for thermal crosstalk reduction in InP-based photonic integrated circuits. J. Lightwave Technol. **32**(24), 4864 (2014)
67. W. Yao, G. Gilardi, N. Calabretta, M.K. Smit, M.J. Wale, Experimental and numerical study of electrical crosstalk in photonic integrated circuits. J. Lightwave Technol. **33**(4), 934 (2015)
68. K. Kato, A. Kozen, Y. Muramoto, Y. Itaya, T. Nagatsuma, M. Yaita, 110 GHz, 50% efficiency mushroom-mesa waveguide p-i-n photodiode for a 1.55 μm wave-length. Photon. Technol. Lett. **6**, 719–721 (1994)
69. J.E. Bowers, C.A. Burrus, Ultrawide-band long-wavelength p-i-n photodetectors. J. Lightwave Technol. **5**(10), 1339–1350 (1987)
70. R. Vetury, I. Gontijo, K. Krishnamurthy, R. Pullela, M.J. Rodwell, High sensitivity and wide-dynamic-range optical receiver for 40 Gbit/s optical communication networks. Electron. Lett. **39**(1), 91–92 (2003)
71. H.G. Bach, Ultra high-speed photodetectors and photoreceivers for telecom and datacom also aiming at THz applications. Proceedings European conference on integrated optics, FB0 (2007)

72. (a) M. Achouche, G. Glastre, C. Caillaud, M. Lahrichi, M. Chtioui, D. Carpentier, InGaAs communication photodiodes: From low- to high-power-level designs. Photon. J. Invited Paper **2**(3), 460 (2010). (b) J. Wei, F. Xia, S.R. Forrest, A high-responsivity high-bandwidth asymmetric twin-waveguide coupled InGaAs-InP-InAlAs avalanche photodiode. IEEE Photon. Technol. Lett. **14**(11), 1590–1592 (2002)
73. K. Shiba, T. Nakata, T. Takeuchi, K. Kasahara, and K. Makita, Theoretical and experimental study on waveguide avalanche photodiodes with an undepleted absorption layer for 25-Gb/s operation. J. Lightwave Technol. **29**(2), 153 (2011)
74. J.C. Campbell, Recent advances in telecommunications avalanche photodiodes. J. Lightwave Technol. **25**(1), 109 (2007)
75. T. Nakata, T. Takeuchi, K. Maliita, Y. Amamiya, T. Kalo, Y. Suzuki, T. Torikai, High-sensitivity 40-Gb/s receiver with a wideband InAlAs waveguide avalanche photodiode. Proceedings European conference on optical commununications, Paper 10.5.1 (2002)
76. K. Makita, T. Nakata, K. Shiba, T. Takeuchi, 40 Gbps waveguide photodiodes. NEC J Adv. Technol. 234–240, Summer (2005)
77. B. Mason, S. Chandrasekhar, A. Ougazzaden, C. Lentz, J.M. Geary, L.L. Buhl, L. Peticolas, K. Glogovsky, J.M. Freund, L. Reynolds, G. Przybylek, F. Walters, A. Sirenko, J. Boardman, T. Kercher, M. Radar, J. Grenko, D. Monroe, L. Ketelsen, Photonic integrated receiver for 40 Gbit/s transmission. Electron. Lett. **38**(20), 1196–1197 (2002)
78. C. Caillaud, P. Chanclou, F. Blache, P. Angelini, B. Duval, P. Charbonnier, D. Lanteri, G. Glastre, M. Achouche, Integrated SOA-PIN detector for high-speed short reach applications. Invited Paper, J. Lightwave Technol. **33**(8), 1596 (2015)
79. P. Angelini, F. Blache, C. Caillaud, P. Chanclou, M. Goix, F. Jorge, K. Mekhazni, J.Y. Dupuy, M. Achouche, Record −22.5 dBm sensitivity SOA-PIN-TIA photoreceiver module for 40 Gb/s applications. IEEE Photon. Technol. Lett. **27**(19), 2027 (2015)
80. M. Anagnosti, C. Caillaud, F. Blache, F. Jorge, P. Angelini, J.F. Paret, M. Achouche, Optimized high speed UTC photodiode for 100 Gbit/s applications. J. Sel. Top. Quantum Electron. **20**(6), 3801107 (2014)
81. M. Anagnosti, C. Caillaud, J.F. Paret, F. Pommereau, G. Glastre, F. Blache, M. Achouche, Record gain × bandwidth (6.1 THz) monolithically integrated SOA-UTC photoreceiver for 100-Gbit/s applications. Invited Paper, J. Lightwave Technol. **33**(6), 1186 (2015)
82. M. Theurer, T. Göbel, D. Stanze, U. Troppenz, F. Soares, N. Grote, M. Schell, Photonic-integrated circuit for continuous-wave THz generation. Opt. Lett. **38**(19), 3724 (2013)
83. L. Shen, Y. Jiao, W. Yao, Z. Cao, J.P. van Engelen, G.C. Roelkens, M.K. Roelkens, M.K. Smit, J.J.G.M. van der Tol, High-bandwidth uni-traveling carrier waveguide photodetector on an InP-membrane-on-silicon platform. Opt. Express **24**(8), 8290–8301 (2016)
84. Y. Tateiwa, M. Takechi, H. Yagi, Y. Yoneda, K. Yamaji, Y. Fujimura, 100 Gbit/s compact digital coherent receiver using InP-based mixer. SEI Tech. Rev. **77**, 59 (2013)
85. S. Farwell, P. Aivaliotis, Y. Qian, P. Bromley, R. Griggs, J.N.Y. Hoe, C. Smith, S. Jones, InP coherent receiver chip with high performance and manufacturability for CFP2 modules. W1I.6, proceedings optical fiber communications conference (2014)
86. R. Stabile, A. Albores-Mejia, A. Rohit, K.A. Williams, Integrated optical switch matrices for packet data networks, Microsys. Nanoeng. Rev. Art. **2**, 15042 (2016)
87. I.M. Soganci, T. Tanemura, K.A. Williams, N. Calabretta, T. de Vries, E. Smalbrugge, M.K. Smit, H.J.S. Dorren, Y. Nakano, Monolithically integrated InP 1 × 16 optical switch with wavelength-insensitive operation. Photon. Technol. Lett. **22**(3), 143–145 (2010)
88. I.M. Soganci, T. Tanemura, Y. Nakano, Integrated phased-array switches for large-scale photonic routing on chip. Laser Photon. Rev. **6**, 549–563 (2012)
89. T. Tanemura, I.M. Soganci, T. Oyama, T. Ohyama, S. Mino, K.A. Williams, N. Calabretta, H.J.S. Dorren, Y. Nakano, Large-capacity compact optical buffer based on InP integrated phased-array switch and coiled fiber delay lines. J. Lightwave Technol. **29**(4), 396–402 (2011)
90. M.J. Kwack, T. Tanemura, A. Higo, Y. Nakano, Monolithic InP strictly non-blocking 8×8 switch for high-speed WDM optical interconnection. Opt. Express **20**(27), 28734 (2012)

91. Q. Cheng, A. Wonfor, R.V. Penty, I.H. White, Scalable, low-energy hybrid photonic space switch. J. Lightwave Technol. **31**(18), 3077–3084 (2013)
92. H. Wang, A. Wonfor, K.A Williams, R.V. Penty and I.H. White, Demonstration of a lossless monolithic 16 × 16 QW SOA switch. Post-deadline paper, proceedings European conference on optical communications (2009)
93. R. Stabile, N. Calabretta, K.A. Williams, Switch-filter wavelength selector: Simulation and experiment. IET Optoelectron. **8**(1), 1–10 (2014)
94. R. Stabile, P. DasMahapatra, K.A. Williams, 4×4 InP switch matrix with electro-optically actuated higher order micro-ring resonators. IEEE Photon. Technol. Lett. Accepted for publication (2016)
95. R. Stabile, N. Calabretta, K.A. Williams, H.J.S. Dorren, Monolithic 16-wavelength selector based on a chain of passband-flattened cyclic AWGs and optical switches. Opt. Lett. **40**(8), 1795–1797 (2015)
96. N. Calabretta, K.A. Williams, H.J.S. Dorren, Monolithically integrated WDM cross-connect switch for nanoseconds wavelength, space, and time switching. Proceedings European conference on optical communications, ID: 0296 (2015)
97. Q. Cheng, R. Stabile, A. Rohit, A. Wonfor, R.V. Penty, I.H. White, K.A. Williams, First demonstration of automated control and assessment of a dynamically reconfigured monolithic 8×8 wavelength-and-space switch. J. Opt. Comm. Networking **7**(3), A388–A395 (2015)
98. M.K. Smit, J. van der Tol, M.T. Hill, Moore's law in photonics. Laser Photon. Rev. **6**, 1–13 (2012)
99. J.J.G.M. van der Tol, R. Zhang, J. Pello, F. Bordas, G.C. Roelkens, H.P.M.M. Ambrosius, P.J.A. Thijs, F. Karouta, M.K. Smit, Photonic integration in indium-phosphide membranes on silicon. IET Optoelectron. **5**(5), 218–225 (2011)
100. wipe. jeppix.eu
101. phastflex. jeppix.eu